Prediction of Induced Voltage on Metallic Pipeline due to AC Power of OHTLs Via a Hybrid Feed-Forward and Radial Basic Function Neural Network

Conference Paper · December 2024

DOI: 10.1109/MEPCON63025.2024.10850418

3 authors, including:

Abdelsalam Hafez Hamza
Benha University (shoubra faculty of Engneering)
93 PUBLICATIONS **245** CITATIONS

2024 25th International Middle East Power System Conference (MEPCON)

Prediction of Induced Voltage on Metallic Pipeline due to AC Power of OHTLs Via a Hybrid Feed-Forward and Radial Basic Function Neural Network

Essam Mohamed A. Shaalan
Electrical Engineering Dept.
Faculty of Engineering at shoubra, Benha University.
Cairo, Egypt
essam.shihata@feng.bu.edu.eg

Mahmoud A. Abbas Elghalban
Orient for Trading and Contracting
Cairo, Egypt
mahmoudabbas8070@gmail.com

Abdel salam H. Hamza
Electrical Engineering Dept.
Faculty of Engineering at shoubra, Benha University.
Cairo, Egypt
abdelsalam.hamza@feng.bu.edu.eg

***Abstract*— Electromagnetic interference (EMI) from high-voltage power systems can significantly jeopardize adjacent conductive structures, such as trains, communication lines, and pipelines, potentially undermining system integrity and operational safety. Accurately predicting the degree of induced voltage is crucial for designing effective mitigation systems for metallic pipelines. Researchers can estimate electromagnetic fields (EMF) with remarkable accuracy in a brief period of time using Artificial Intelligence (AI) techniques. Three Artificial Neural Network (ANN) models are introduced in this paper that were created to estimate the voltage induced by AC power from Overhead Transmission Lines (OHTLs) in pipelines. The models were trained on a dataset of pipeline-induced voltage measurements and OHTLs parameters to predict the induced voltage based on these features. The models include a Feed-Forward Neural Network (FFNN), a Radial Basis Function Neural Network (RBFNN), and a Hybrid Neural Network (HNN). A sensitivity analysis was performed on the hyper-parameters of these models to identify the ideal configuration for enhanced accuracy and response time. The HNN model significantly outperformed FFNN and RBFNN in predicting pipeline-induced voltage, demonstrating an impressive decrease of 90.92848% and 56.59041% within Root-Mean-Squared Errors (RMSE), respectively. This makes HNN model a promising choice for pipeline-induced voltage prediction, outperforming methods proposed in other recent studies. After training, the model is tested with a separate dataset, and its accuracy and speed for new data points are evaluated. The model can predict induced voltage with nearly 97.15% accuracy within 15 milliseconds. These results show that the hybrid method outperforms existing AI-based techniques, with sensitivity analysis revealing that HNN models with hidden layers of triple and double are the most effective for pipeline-induced voltage prediction.**

Keywords*— *Electromagnetic interference, Artificial intelligence, Induced voltage, AC power, OHTLs, Root Mean Squared Error and Prediction.

I. INTRODUCTION

The fast economic development in many countries has resulted in a constantly increasing need for basic supplies, essential energy resources, and electricity. To address the increasing demand, it is imperative to augment current high-voltage OHLs and gas, fluid, as well as oil delivery pipes, or to establish new ones. Consequently, high-voltage OHLs are frequently constructed in conjunction with common transmission and distribution corridors that also transport fluids like gas, and oil via pipelines. These OHLs comprise conductors that convey alternating current (AC) from power production facilities to distribution centers and end-users. The complex EMF pattern is formed by the electrical and magnetic fields generated by the current flow through these conductors, which are located around the transmission line [1-6].

Estimating EMF is critically important for several reasons. The primary concern is its significant impact on human health. Numerous studies over recent decades have linked EMF exposure from OHLs in residential areas to an increased risk of cancer, particularly childhood leukemia. Additional research has indicated an increased risk of brain cancers in those subjected to extended, high-intensity EMF. Pipelines are susceptible to high induced currents and voltages as a result of EMI from OHLs as they occupy the same right-of-way [7-10].

Without having an immediate electrical link, EMI is occasionally conveyed from OHTLs to neighboring structures of metal. The OHLs emit electromagnetic fields, which induce AC interference in surrounding metal-based liquids such as gas and oil pipes. This makes metallic pipes, whether above or below ground, susceptible to induced excessive AC potentials and currents. The situation is exacerbated when metal pipelines are positioned near OHLs instead of an electrical link to a mitigation system designed to lower induced voltage levels. In severe circumstances, particularly during OHL failures, the voltage generated on unsafe metal pipelines can reach several thousand volts [11].

979-8-3503-7964-8/24/$31.00 ©2024 IEEE

AC interference coupling techniques are divided as capacitive, inductive, or conductive couplings based on circuit configuration. When huge amounts of current are discharged into the ground, conductive coupling develops as a result of the ground voltage rise, notably at OHL, substation, and energy plant grounding systems. This form of coupling is a big hazard throughout power system outages, particularly when metal pipelines are adjacent OHLs.

Magnetic fields cause inductive coupling. OHLs transporting huge currents generate significant magnetic fields in their surroundings, which can induce voltage in nearby metallic objects via magnetic field coupling. Factors influencing this form of connection include the present level of the OHLs, the length of parallel between the OHLs and metallic components, and their distance from each other.

Capacitive coupling arises from a potential variation among two systems. The variation in voltage across OHLs as well as any adjacent structure which can be conductive, especially those made of metal pipeline, creates a field of electricity across the two structures [12].

Calculating AC-induced currents as well as voltages on metal fluids supply pipelines near OHLs is difficult due to the intricate interactions involved. These interactions are typically explained using differential equations which simulate coupling processes and EMF. These equations are usually solved with specific assessment methods like the method known as Finite Difference (FDM) as well as Finite Element (FEM).

FEM, in particular, converts the intricacies of EMI to modelling using numerical methods. However, as the number of mesh elements and parameters to be evaluated increases, the computational cost and complexity of the simulation also rise significantly. Each new problem geometry requires fresh mesh discretization and evaluation, which adds to the computational burden. Evaluating EMI that exists between high-voltage OHLs and metal fluids pipelines using FEM demands considerable computational power and time, especially for various system configurations. As a result, there has been growing interest in predictive approaches that can accurately estimate the required information from a variety of issue designs without requiring of extensive simulations [13].

Since the early 21st century, Engineering and physics researchers have embraced AI techniques in growing numbers since the early 2000s. These techniques are especially well-suited for EMF estimation, as they can effectively handle intricate data sets, deliver precise estimations, and come with numerous benefits throughout conventional methods. AI models can be continuously improved by retraining them with new data, expanding their accuracy and adaptability to various conditions. Among the various AI methods, Artificial Neural Networks (ANNs) are particularly well-regarded for solving engineering and physics problems. Drawing inspiration from the brain of human, ANNs are versatile and adaptable models capable of learning from both small and enormous sets and extracting valuable findings from massive volumes of data. Their ability to manage relationships that are not linear has made them especially useful for dealing with complicated and changing challenges. Furthermore, ANNs can predict desired characteristics with great precision in just a brief amount of time. FFNN represents one of foremost frequently employed techniques for ANN stipulated that to its ease of use and precision; however, another variant of ANN, the RBFNN, introduces additional complexity by processing inputs differently, offering an alternative approach to prediction tasks [14,15].

The HNN is significant in prediction tasks because it combines the strengths of different neural network architectures, leading to enhanced performance and accuracy compared to traditional models. While FFNNs are known for their simplicity and effectiveness in handling straightforward prediction problems, and RBFNNs add complexity by processing inputs differently to capture more intricate patterns, HNNs take this a step further by integrating multiple neural network approaches within a single framework. This integration allows HNNs to leverage the unique advantages of each network type, such as the ability of FFNNs to handle linear relationships and the capability of RBFNNs to model non-linear patterns more effectively.

While previous attempts to assess or quantify EMF adjacent OHTLs, there is still a significant gap between researchers regarding the establishment of a rapid, accurate, empirical evidence technique for estimating these fields, rather than relying solely on traditional mathematical techniques. FFNN has been the predominant choice for EMF estimation in recent research, but often falls short in terms of accuracy. Given these restrictions, there is a clear need for a more sophisticated model that can properly addressing extremely nonlinear data. The HNN model stands out as one of the most effective artificial intelligence models, known for its precision in predicting complex and nonlinear problems. In prediction tasks, particularly those involving intricate and dynamic datasets, HNNs have demonstrated superior accuracy compared to RBFNNs and FFNNs. The hybrid structure of HNNs allows them to adapt more effectively to various data types and capture subtle dependencies that single-model networks might overlook, leading to more accurate predictions. HNNs have shown significant reductions in prediction errors when compared to RBFNNs and FFNNs. This paper proposes the use of HNN models to estimate the induced voltage of OHTLs. Sensitivity analysis has been conducted on these models to determine the best parameters for training, ensuring they achieve the highest accuracy and stability. Hence, The models will be explained and thoroughly described before moving on to a description of the sensitivity study procedure. The findings of each phase of the sensitivity study are illustrated in Section 3 and compares the performance characteristics of the FFNN, RBFNN, and HNN models. In the end, Section 4 will provide a brief conclusion.

II. ANN METHODS

In this work, ANN was selected for this study due to its remarkable flexibility in handling various datasets. Whether

979-8-3503-7964-8/24/$31.00 ©2024 IEEE

dealing with large data sets containing numerous data points and influential variables, or fewer datasets with a few findings that may not be appropriate for complicated machine learning algorithms, ANN proves to be highly adaptable. A specific variant of ANN, the HNN, was chosen as the primary approach for this research. For comparison purposes, two other widely-used methods, the FFNN and the RBFNN, were also employed. The following sections will discuss these methods in detail and highlight their differences.

A. Feed Forward Neural Network (FFNN)

A.1 Architecture

FFNN is a basic form of ANN which is composed of a layer act as input, one or more layers that are hidden, in addition a layer called output. This kind of structure allows data to travel in a single path through the input phase layer to the final layer, with no feedback. Every individual neuron in the currently operating layer connects to every neuron in subsequent layer, and these connections having assigned weights. Each neuron receives activation functions, which introduce nonlinearity and allow the network to model complicated interactions between input and output data.

A.2 Fundamental Equations of FFNN Methodology

The core principles underlying FFNN functioning involve linear combinations of inputs, activation functions, and error minimization through backpropagation [16].

A.2.1 Linear Combination:

For each neuron j in a layer, the output z_j is calculated as:

$$z_j=\sum_{i=1}^{n} w_{ij}x_i + b_j \quad (1)$$

where x_i relates to the neuron's inputs, w_{ij} are the weights which are connected with the inputs, and b_j is the bias component for neuron j.

A.2.2 Activation Function:

The neuron output a_j is then passed through an activation function $f()$ [16]:

$$a_j=f(z_j) \quad (2)$$

The logistic functioning, trigonometric functions, as well as Rectified Linear are all prevalent functions associated with activation.

A.2.3 Output Calculation:

The output layer aggregates the outputs of its neurons to generate the final prediction y [16].

$$y = f(\sum_{i=1}^{m} w_{0ij}x_i + b_0) \quad (3)$$

where w_{0ij} are the weights connecting the hidden layer neurons to the output layer neurons, as and b_0 represents output layer bias.

A.2.4 Error Function:

The error (E) is calculated as the variation in between the expected output (y) and the real target (t). A popular error indicator is the mean square errors (MSE) [16]:

$$E = \frac{1}{2}\sum_{k=1}^{N}(y_k - t_k) \quad (4)$$

since N denotes the entire set of training sets.

A.2.5 Backpropagation:

Weights are manipulated using the descending gradient method to minimize the error function [16]:

$$w_{ij} = w_{ij} - \eta\frac{\partial E}{\partial w_{ij}} \quad (5)$$

where η provides the rate of learning, and $\frac{\partial E}{\partial w_{ij}}$ indicates the error gradient with regard to the weights.

A.3 Training, Validation, and Testing Processes for FFNN

In the training process, the set of data gets split into three separate portions, firstly learning sets, secondly validation sets, and last sets for testing. During forward pass, inputs are passed through the network to generate predictions. The loss is then calculated by evaluating the variation in between the expected and real values using an error function. Backpropagation backwards the error backward through the designed network, allowing for weight adjustments to minimize the error. This technique is performed for several times until the model meets or reaches a stopping criterion.

Throughout the validation procedure, the model is tested on the set of validation data to ensure that it performs well and does not overfit. The validation findings can be applied to fine-tune major parameters including g rate of learning, size of layers that are hidden, and the total number of neurons.

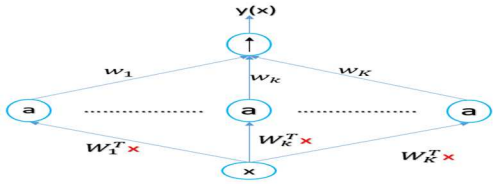

Fig. 1. Diagrammatic representation of FFNN.

After training, the model is tested on an unseen test set to determine its capacity for generalization capabilities. Evaluation metrics like as RMSE and degree of correlation (R-squared or R^2) are used to rate the model's accuracy in predicting EMF amounts. The network's operational features are fine-tuned across numerous rounds employing optimization algorithms such as Levenberg-Marquardt, that utilize a particular portion of the data used for training to determine updates necessary to the weights and biases. Figure 1, show diagrammatic representation of FFNN.

B. Radial Basic Function Neural Network (RBFNN)

B.1 Architecture

979-8-3503-7964-8/24/$31.00 ©2024 IEEE

RBFNN consists of three stages of layers: input, then hidden, and lastly output. The layer that is hidden utilizes an intricate role of transfer, commonly a Gaussian function, while its output layer applies the linear function of transfer. The input layer is made up of nodes that serve as sources linked to the hidden layer via weighted links. Neurons in hidden layer apply RBFNN, where each neuron computes a function based on the distance from a central point—this is a defining characteristic of RBFNNs. The network's output produces a linear mixture of the hidden layer outputs, allowing it for approximation complex functions. RBFNNs are trained using a supervised gradient-descent method, where the network's parameters (centers, widths, and weights) are adjusted to minimize the error function. The model's efficacy is evaluated using an additional validation dataset to assess its capacity to adapt to new data. Performance metrics like Mean Absolute Error (MAE), RMSE, and R-squared are utilized to evaluate how well the RBFNN performs. Finally, the network's predictive accuracy is tested on a separate dataset, with results compared to observed data using the same statistical measures as in the validation phase. Figure 2, show Diagrammatic representation of RBFNN.

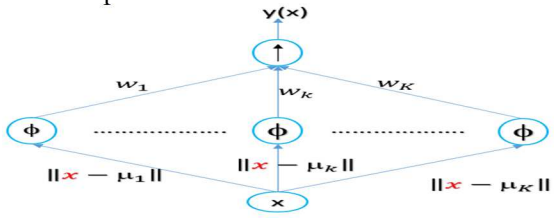

Fig. 2. Diagrammatic representation of RBFNN.

B.2 Fundamental Equations of RBFNN Methodology

RBFNN approach is based on the following principal components: the input layer, hidden layer involving radial base functions, and output layer. The following is a breakdown of the essential equations [17]:

B.2.1 Input to Hidden Layer Transformation:

The vector that is input X is fed inside the network. The hidden layer applies a radial basis function $\phi_j(x)$ to each neuron j.

A commonly used radial basis function is the Gaussian function:

$$\phi_j(x) = \exp(-\frac{\|X-c_j\|^2}{2\sigma_j^2}) \quad (6)$$

Where C_j is the center of RBF for neuron j, σ_j is the spread of the RBF, and $\|X - C_j\|$ is the Euclidean distance throughout the vector that is input X as well as the center C_j.

B.2.2 Transforming an unseen layer into a final layer:

The network's output y_i is the weighted combined amount of the outputs from the hidden layer:

$$y_i=\sum_{j=1}^{M} w_{ij}.\ \phi_j(x) + b_i \quad (7)$$

Where w_{ij} denotes the weight linking the *j-th* hidden neuron with the *i- th* output neuron, b_i denotes the term that describes the bias for the *i- th* output neuron and M is the overall number of hidden neurons.

B.2.3 Training (Parameter Adjustment):

The points in centerC_j are chosen utilizing techniques such as K-means clustering or can be learned directly during training. Widths σ_j are often set as a function of the distance between centers or can be tuned during training. The weights w_{ij} are typically adjusted employing a supervised method to learning such as descent by gradient or the least squares method to minimize error function, typically MSE:

$$MSE = \frac{1}{2}\sum_{i=1}^{N} (y_i^{pred} - y_i^{true})^2 \quad (8)$$

Where y_i^{pred} is the predicted output by the network, y_i^{true} is the actual target output, and N represents the total amount of training samples.

B.2.4 Output Calculation:

Final output y of the RBFNN for a given input x is:

$$y = W^T.\Phi(X)+b \quad (9)$$

Where W^T represents the dimension of the weight structure, $\Phi(X)$ is the vector which represents RBF final results, and b denotes a bias vector data.

C. Hybrid Neural Network (HNN)

The architecture of HNN combines RBFNN with FFNN to enhance prediction accuracy for pipeline-induced voltage caused by AC power from OHTLs.

In this architecture, the RBFNN functions as the initial layer, transforming the input features to detect non-linear correlations among parameters like voltage, current, and the output (induced voltage). The RBFNN employs a Gaussian function for this transformation, which effectively handles complex data patterns.

After the RBFNN processes the features, they are passed to the FFNN, which consists of three hidden layers. These layers further refine the data, enabling the FFNN to learn deeper patterns and relationships. This multi-layer structure enhances model's predictive capabilities.

By integrating non-linear transformation of the RBFNN with the deep learning structure of the FFNN, the HNN provides superior performance in predicting pipeline-induced voltage, offering a robust solution for complex electrical systems.

979-8-3503-7964-8/24/$31.00 ©2024 IEEE

III. SYSTEM MODELING

Pipeline under study is an outgrowth of a prior research work presented in [18]. This pipeline is owned by Egypt's Fayoum Gas Agency. This study provides a supplemental investigation of the pipeline's induced AC voltage. A real-life example of the Fayoum gas pipeline is examined. The 72-kilometer pipeline travels parallel to or crosses several transmission lines (El-Kurimate, Samaloute, in addition Dimo electricity lines, October 6th), as illustrated in Figure 3. Two of them are 500 kV lines, and the other is a 220 kV line. The 500 kV TL towers are equipped with three-phase power circuits and two earth cables, whereas the 220 kV tower has twinned a three-phase electricity circuits in addition to an earth wire. TL belongs to El-Kurimate is 124 km long and can transmit 575 MVA of power. The Samaloute TL has a power rating of 1000 MVA and is 209 km long. In addition to TL of The Dimo-6th of October is 90 km long and has in every single circuit a rated power of 158 MVA. Study pipeline measures 0.4064 m in diameter and is coated with high-density polyethylene. The protective coating measures 4 mm thick and has a resistance of $10^6 \Omega/m^2$. The pipeline is buried at 1.5m deep in soil with resistance varying from 2500 to 100 ohmmeters, as per the arrangement. Technical data, configuration of the three transmission lines, distance of separation in between the gas pipeline and the three TLs and resistance of soil at each kilometer of the whole samples (77 samples for actual measurements for separation distances, soil resistivity and pipeline induced voltages) is presented in [18].

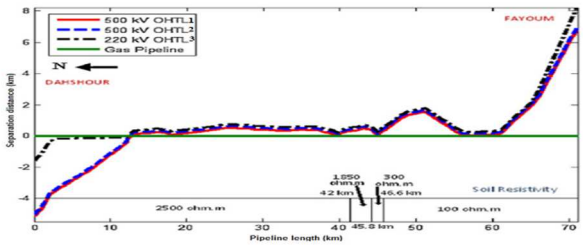

Fig. 3. Configuration of Fayoum Gas Company's pipeline with three power lines [18].

By applying the ANN methods described in the previous sections to this case study, this paper able to accurately predict pipeline-induced voltage. Subsequently, this paper compared the performance of the best-performing ANN model to the actual measurements of this case in [18] as well as the traditional mathematical methods (Nodal Network Analysis NNA) to assess its effectiveness in predicting induced voltage.

IV. RESULTS AND DISCUSSION

A. Error Metrics for Evaluating Model

To analyze an estimation precision of created models, various assessment metrics have been employed, including U-statistic, RMSE, absolute error, MAPE, RACF, and R-squared. The mathematical formulations for these metrics are provided below [19,20]:

$$MAPE\% = \frac{1}{N}\sum_{t=1}^{N}\frac{|(EP(t)_{actual} - EP(t)_{estimated})|}{EP(t)_{actual}} \text{x}100 \quad (10)$$

$$\text{RMSE} = \sqrt{\sum_{k=1}^{n_s}\frac{(d_k - y_k)^2}{n_s}} \quad (11)$$

$$U = \frac{RMSE}{\sqrt{\frac{1}{N}\sum_{t=1}^{N}(EP(t)_{actual})^2} + \sqrt{\frac{1}{N}\sum_{t=1}^{N}(EP(t)_{estimated})^2}} \quad (12)$$

$$\text{RACF} = \frac{|\sum_{t=2}^{N}(e(t)\, e(t-1))|}{\sum_{t=1}^{N}(e(t))^2} \quad (13)$$

$$R^2 = \frac{\sum_{k=1}^{n_s}(d_k - \bar{d})\,(y_k - \bar{y})}{\sqrt{\sum_{k=1}^{n_s}(d_k - \bar{d})^2 \sum_{k=1}^{n_s}(y_k - \bar{y})^2}} \quad (14)$$

Where N denotes the total number of rounds for every built, y represents the predicted magnitude, $\bar{y}$ indicates the mean amount for x in N rounds, ns represents the total number of samples used in training, dk denotes the real value, and $\overline{dk}$ provides the mean amount of dk.

These metrics are essential for evaluating the performance of neural network models. MAPE% assesses the average percentage error in predictions, while RMSE focuses on the magnitude of errors, particularly emphasizing larger ones. The U-statistic, ranging from zero to one, compares the model's predictions to a naive baseline—values nearer to the value one suggest that the model performs not better as a basic projection, while values nearer to a zero indicate better precision and fitness. RACF analyzes the correlation of residuals to identify unmolded patterns, with values typically between zero and one; a significant deviation from zero suggests the presence of patterns outside a confidence level. Lastly, R-squared indicates the proportion of deviation in the target parameter which the model explains, indicating its overall effectiveness.

B. Parameter Settings of Applied Methods

Table I distils parameters for every one of the techniques used in this investigation.

TABLE I. CONFIGURATION OF IMPLEMENTED TECHNIQUES' PARAMETERS.

Methods	Parameters	Value
FFNN	Hidden layer	3
	Transfer Function	Logistic functioning, trigonometric functions, as well as rectified linear are all prevalent functions associated with

Methods	Parameters	Value
		activation. Such functions provide nonlinearity, which allows the network to simulate complicated operations.
	Learning Algorithm	Backpropagation is combined with an improvement procedure, like Decent of Gradient as well as Levenberg-Marquardt, to reduce the gap among estimated and real results by adjusting weights.
RBFNN	Hidden layer	3
	Transfer Function	The Gaussian function measures the gap in between the input data and the neuron's center. This function helps in addressing patterns that are not linear within datasets.
	Learning Algorithm	Two-step process: first, the centers of the radial basis functions are determined, often using techniques like K-means clustering; second, the output weights are optimized using methods like linear regression or gradient descent.
HNN	Hidden layer	combines the hidden layers of both RBFNN and FFNN. RBFNN's hidden layer captures non-linear relationships in the data, while the FFNN's hidden layers further refine the input by learning deeper patterns and dependencies.
	Transfer Function	Gaussian transfer function in the RBFNN component for non-linear transformation and functions like Sigmoid or ReLU in the FFNN component for further processing of the transformed data.
	Learning Algorithm	A combination of techniques used in RBFNN and FFNN. The RBFNN component is trained first, followed by the FFNN, using backpropagation or other advanced optimization methods to fine-tune the overall model for better accuracy.

C. Model Sensitivity and Hyper-Parameters

Analyzing sensitivity is crucial because it helps ensure that the final model is reliable. If the model is well-tuned with the right hyper-parameters, it can predict pipeline induced voltage with high accuracy [21].

C.1 Size of hidden layers as well as neurons

This research, three different configurations of hidden layers were tested. It started with just one layer and went up to three layers. This testing helps them to find the optimal size of hidden layers during their specific set of data. The study looked at the performance of each configuration to decide which one worked best. It considered the number of neurons (the basic units of the ANN) in each hidden layer. This helps the study make an informed decision about which setup to use for further analysis.

Figure 4 illustrates that for the HNN, raising the size of hidden layers leads to most effective performance, as indicated by the lowest error rates based on RMSE. The RBFNN also shows strong performance in both RMSE and R-Squared, especially with additional layers. In contrast, while FFNN performs adequately, it is surpassed by the other models as the complexity of the network increases.

Table II presents the optimal neuron configuration for each layer based on the RMSE value. The results imply that HNN of triple-layer design using a neuron structuring of 15 neurons in first layer, 10 neurons in the second and 5 neurons in the last achieves the best performance due to its exceptionally low RMSE.

C.2 Training and Activation Functions

The study evaluates the performance of four widely recognized training functions frequently referenced in the literature. The Levenberg-Marquardt (LM) method is an optimization technique commonly employed in neural networks, recognized for its rapid convergence and precision,

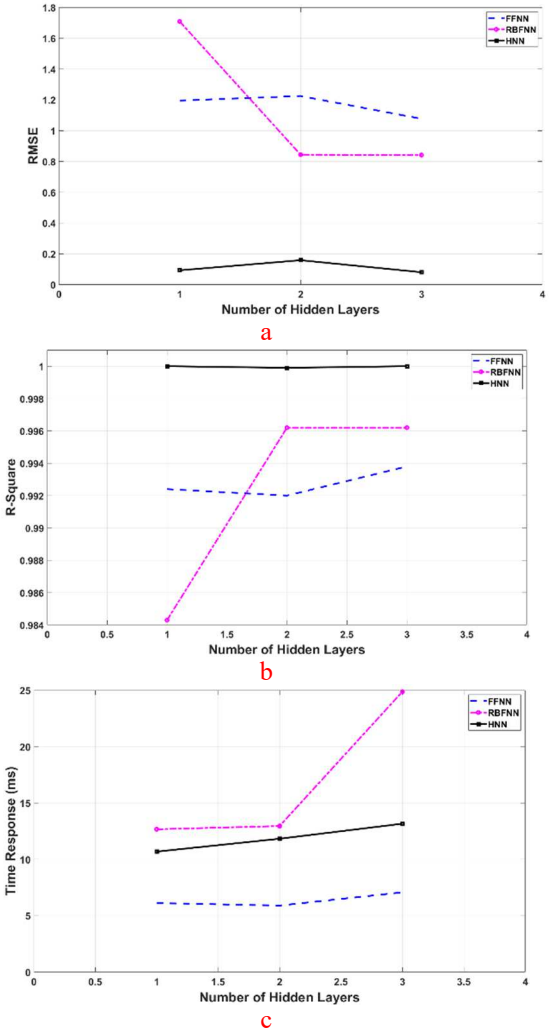

Fig. 4. Evaluating the size of hidden layers in FFNN, RBFNN, and HNN to predict pipeline induced voltage. (a) RMSE; (b) R-squared; and (c) speed of response.

TABLE II. SIZE OF LAYERS AND NEURONS OF IMPLEMENTED TECHNIQUES.

Assessment of Layers and Neurons Size for FFNN Prediction of Induced Voltage			
Layers Size	1	2	3

Assessment of Layers and Neurons Size for FFNN Prediction of Induced Voltage			
Neurons Size	15	[7 7]	[15 10 5]
MAPE	19.1447	17.994	10.78
RMSE	1.1952	1.2246	1.0769
AbsError	0.8774	0.88	0.6217
Ustatistic	0.1226	0.1256	0.1105
R-Squared	0.9924	0.992	0.9938
Response Time (ms)	6.121	5.9	7.074

Assessment of Layers and Neurons Size for RBFNN Prediction of Induced Voltage			
Layers Size	1	2	3
Neurons Size	15	[7 7]	[15 10 5]
MAPE	19.0304	9.7042	7.0452
RMSE	1.7083	0.8438	0.8418
AbsError	1.1048	0.5876	0.5377
Ustatistic	0.1752	0.0865	0.0863
R-Squared	0.9843	0.9962	0.9962
Response Time (ms)	12.668	12.949	24.868

Assessment of Layers and Neurons Size for HNN Prediction of Induced Voltage			
Layers Size	1	2	3
Neurons Size	15	[7 7]	[15 10 5]
MAPE	3.1078	3.4453	2.6759
RMSE	0.0933	0.1589	0.0808
AbsError	0.0648	0.0984	0.0342
Ustatistic	0.0096	0.0163	0.0083
R-Squared	1	0.9999	1
Response Time (ms)	10.684	11.827	13.16

especially in small to medium-scale tasks. Scaled Conjugate Gradient (SCG) is an effective second-order technique that enhances training efficiency while reducing memory consumption. Resilient Backpropagation (RB) enhances gradient-based learning by modifying weight updates to facilitate swifter and more precise training. Finally, Variable Learning Rate Backpropagation (VLRB) adjusts the pace of learning actively during training to achieve an equilibrium between convergence speed as well as stability. These functions are crucial for optimizing the training process of neural networks and include variations that have been extensively tested to determine their effectiveness. Each function employs a unique approach to adjust the biases as well as weights throughout the predictive network during the learning phase, ultimately influencing the overall accuracy and generalization ability of the model. The selection of these specific training functions is based on their popularity and proven effectiveness in various applications, making them ideal candidates for comparative analysis in this study.

Figure 5 illustrate that, the LM training function achieves the smallest RMSE in addition greatest R-squared values. Additionally, HNN model outperforms FFNN and RBFNN models in terms of RMSE when using the LM, SCG, and VLRB training functions. However, the ideal design of the HNN model provides a longer speed time than the two techniques. Nevertheless, the HNN technique consistently delivers better precise findings across most training functions. As a result, the HNN model trained with the LM function is considered the best model at this stage.

The FFNN typically uses a combination of nonlinear activation functions to introduce nonlinearity inside the algorithm, thus permitting it to learn intricate designs. Popular activation techniques used in FFNN involve [19]:

Log-sigmoid $$F(x) = \frac{1}{1+\exp(-x)} \quad (15)$$

Tanh $$F(x) = \tanh x \quad (16)$$

Saturated Linear $$F(x) = \begin{cases} 0 & x < 0 \\ 1 & x > 0 \end{cases} \quad (17)$$

Log-sigmoid $$F(x) = \frac{1}{1+\exp(-x)} \quad (18)$$

Pure line $$F(x) = x \quad (19)$$

The Gaussian function (mentioned in equation number (6)) is implemented in RBFNN to capture local patterns [22].

The HNN model integrates features from both RBFNN and FFNN to harness their respective advantages. It employs Gaussian activation functions in the hidden layer, like RBFNN, to identify localized patterns within the input data. For additional hidden layers or output layers, it utilizes log-sigmoid, Tanh, saturated linear, or pure-line functions, similar to FFNN, to introduce nonlinearity and capture complex patterns across the entire input space. This blend of activation functions enables the HNN to benefit from the RBFNN's ability to detect localized features and the FFNN's capability for global learning, resulting in a more adaptable and effective model for handling complex data.

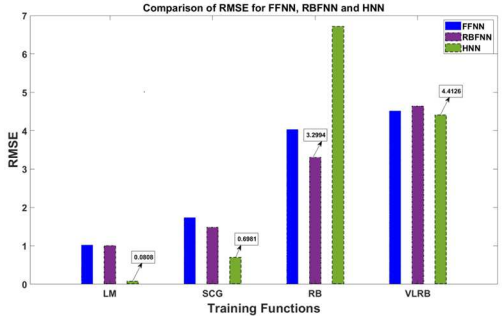

a

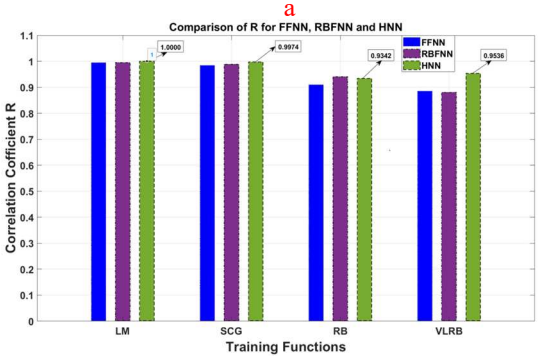

b

979-8-3503-7964-8/24/$31.00 ©2024 IEEE

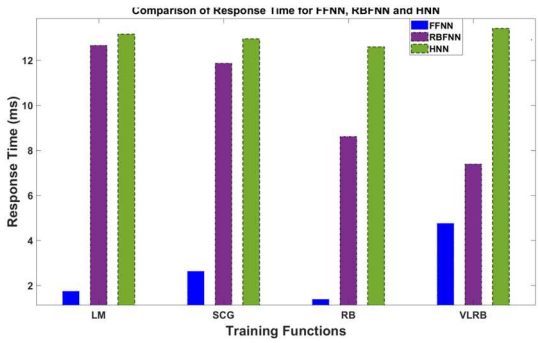

c

Fig. 5. Training Functions Analysis for FFNN, RBFNN, and HNN triple-layer designs for pipeline induced voltage. (a) RMSE (b) R (c) Speed time.

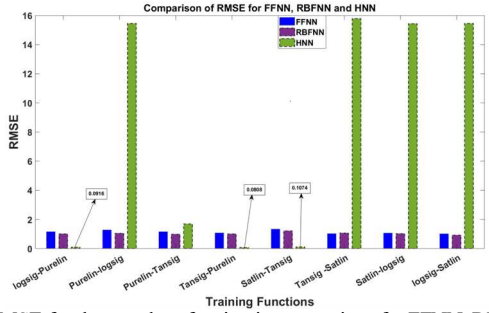

Fig. 6. RMSE for the couples of activation operations for FFNN, RBFNN, and HNN for pipeline induced voltage.

Tansig–Purelin and Logsig–Purelin activation function pairs for the HNN produced the lowest RMSE values are illustrated in Figure 6. This indicates that the HNN provides more accurate estimates of pipeline-induced voltage for three combinations of activation functions.

V. COMPARISON WITH PREVIOUS STUDIES

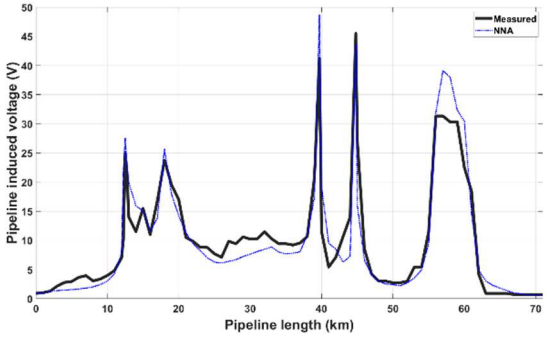

a

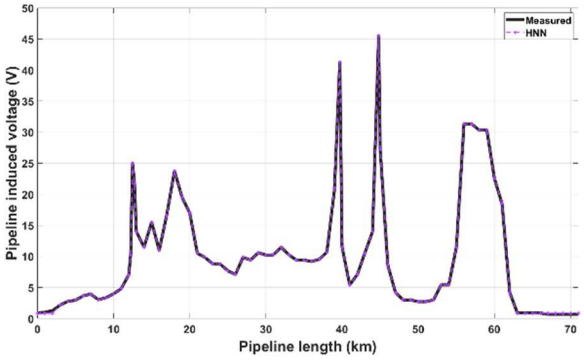

b

Fig. 7. Pipeline induced voltage. a) NNA method and actual measurements. b) HNN method and actual measurements.

This part compares the precision of the model suggested in the current research with NNA used in the study referenced in [23] and compares them with the actual measurements in [18]. According to Table III, the model suggested has the lowest RMSE among published studies. Furthermore, as demonstrated in Figures 7 and 8, the relative error on this paper never exceeded 2.6759% (in the worst case), whereas other studies reported errors up to 28.5809%.

TABLE III. PRECISION OF THE HNNN DESIGNED MODEL AGAINST OTHER WORKS (ANN).

Performance Indexes	Method	
	HNN	NNA
MAPE (%)	2.6759	28.5809
RMSE	0.0808	3.37
Absolute Error	0.0342	2.2331
U-Statistic	0.0083	0.2359
RACF	0.3912	0.4099

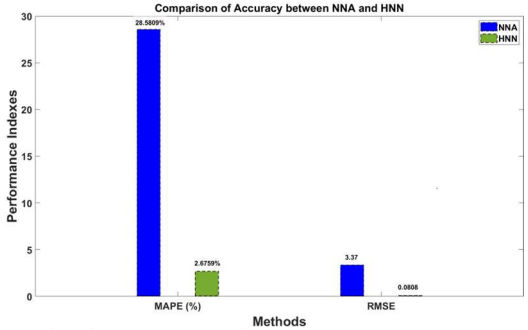

Fig. 8. Comparison between NNA and HNN accuracy.

CONCLUSIONS

In this investigation, hybrid model incorporating RBFNN and FFNN has been developed for estimating induced voltage

on metal pipelines located within the right-of-way of OHTLs. The primary objective was to create a fast, cost-effective implementation using AI techniques based on neural networks.

The proposed HNN demonstrated superior accuracy compared to the more commonly used FFNN and RBFNN models. Notably, the training time for the HNN was under 14 milliseconds, and its response time was less than 14 milliseconds on standard personal computer, highlighting its suitability for real-time applications. Although the HNN model features an extra intricate design, it achieved nearly twice a process time of FFNN while delivering significantly greater precision.

References

[1] A. M. Sayed, A. M. Ahmad, S. A. Ward, and E. M. Shaalan, "Improved prediction of ion mobility for precipitators using FDM-FMG on fine computational domains," Electric power systems research, vol. 214, Cairo, Egypt, January 2023.

[2] E. M. Shaalan, M. A. Mostafa, A. S. Hamza, and M. Al-Gabalawy, "Cathodic Protection Performance Improvement of Metallic Pipelines based on Different DC Compensation Methods," Electric power systems research, vol. 210, pp. 108064-, Cairo, Egypt, September 2022.

[3] M. A. Mostafa, M. Al-Gabalawy, E. M. Shaalan, and A. S. Hamza, "Mitigation of the AC corrosion of the metallic pipelines using the hydroxide and solid-state polarization cells; A comparative study," Electric power systems research, vol. 202, pp. 107585-, Cairo, Egypt, January 2022.

[4] E. M. Shaalan, S. A. Ward, and A. Youssef, "Analysis of a Practical Study for Under-Ground Cable Faults Causes," in 2021 22nd International Middle East Power Systems Conference (MEPCON), IEEE, Cairo, Egypt, 2021, pp. 208–215.

[5] M. A. Mostaf, M., M. Al-Gabalawy, E. M. Shaalan, and A. S. Hamza, "Different Polarization Cells Based for Mitigating theAC Induced Voltages on the Metallic Pipeline," Engineering Research Journal (Shoubra), vol. 50(1), pp. 126-134, Cairo, Egypt, October 2021.

[6] E. M. Shaalan, S. A. Ward, and A. Youssef, "Effect of cavity position, size and geometry on partial discharge behaviour inside 18/30 kv xlpe cables," International journal on electrical engineering and informatics, vol. 13, no. 2, pp. 495–507, Cairo, Egypt, June 2021.

[7] O. Ituabhor, J. Isabona, J.T. Zhimwang, and I. Risi, "Cascade Forward Neural Networks-based Adaptive Model for Real-time Adaptive Learning of Stochastic Signal Power Datasets," International Journal of Computer Networks and Information Security, vol. 3, pp. 63–74, Lokoja, Nigeria, June 2022.

[8] L. Wan, S. Negri, G. Spadacini, F. Grassi, and S. A. Pignari, "Enhanced Impedance Measurement to Predict Electromagnetic Interference Attenuation Provided by EMI Filters in Systems with AC/DC Converters," Applied sciences, vol. 12, no. 23, pp. 12497-, Milan, Italy, December 2022.

[9] G. Lucca, L. Sandrolini, A. Popoli, M. Simonazzi, and A. Cristofolini, "Assessment of AC Corrosion Probability in Buried Pipelines with a FEM-Assisted Stochastic Approach," Applied sciences, vol. 13, no. 13, pp. 7669-, Bologna, Italy, June 2023.

[10] A. Z. E. Dein, O. E. Gouda, M. Lehtonen, and M. M. F. Darwish, "Mitigation of the Electric and Magnetic Fields of 500-kV Overhead Transmission Lines," IEEE access, vol. 10, pp. 33900–33908, Cairo, Egypt, March 2022.

[11] Mingyang Lu, Wenqian Zhu, Liyuan Yin, A. J. Peyton, Wuliang Yin, and Zhigang Qu, "Reducing the Lift-Off Effect on Permeability Measurement for Magnetic Plates From Multifrequency Induction Data," IEEE transactions on instrumentation and measurement, vol. 67, no. 1, pp. 167–174, U.K, January 2018.

[12] A. K. Thakur, A. K. Arya, and P. Sharma, "The science of alternating current-induced corrosion: a review of literature on pipeline corrosion induced due to high-voltage alternating current transmission pipelines," Corrosion reviews, vol. 38, no. 6, pp. 463–472, Dehradun, India, November 2020.

[13] R. Kafafy, T. Lin, Y. Lin, and J. Wang, "Three-dimensional immersed finite element methods for electric field simulation in composite materials," International journal for numerical methods in engineering, vol. 64, no. 7, pp. 940–972, U.S.A, August 2005.

[14] L. Czumbil, D. D. Micu, D. Stet, and A. Ceclan, "A neural network approach for the inductive coupling between overhead power lines and nearby metallic pipelines," in 2016 International Symposium on Fundamentals of Electrical Engineering (ISFEE), IEEE, Bucharest, Romania, July 2016.

[15] R. Kumar, S. Srivastava, and J. R. P. Gupta, "Modeling and adaptive control of nonlinear dynamical systems using radial basis function network," Soft computing (Berlin, Germany), vol. 21, no. 15, pp. 4447–4463, New Delhi, India, 2017.

[16] Yagawa, G. and A. Oishi (2021). Feedforward Neural Networks. Computational Mechanics with Neural Networks. Cham, Springer International Publishing: 11-23.

[17] I. Ladlani, L. Houichi, L. Djemili, S. Heddam, and K. Belouz, "Modeling daily reference evapotranspiration (ET0) in the north of Algeria using generalized regression neural networks (GRNN) and radial basis function neural networks (RBFNN): a comparative study," Meteorology and atmospheric physics, vol. 118, no. 3–4, pp. 163–178, Algeria, July 2012.

[18] E. H. M. G. Mohamed, "Evaluation of Electrical Interference from High Voltage Transmission Lines to Metal Pipelines and Corrosion Problem," A Thesis, Faculty of Engineering, Helwan University, March 2018.

[19] S. Hr Aghay Kaboli, A. A. Hinai, A. H. Al-Badi, Y. Charabi, and A. Al Saifi, "Prediction of metallic conductor voltage owing to electromagnetic coupling via a hybrid ANFIS and backtracking search algorithm," Energies (Basel), vol. 12, no. 19, pp. 3651-, Muscat, Oman, September 2019.

[20] S. Alipour Bonab, W. Song, and M. Yazdani-Asrami, "A New Intelligent Estimation Method Based on the Cascade-Forward Neural Network for the Electric and Magnetic Fields in the Vicinity of the High Voltage Overhead Transmission Lines," Applied sciences, vol. 13, no. 20, pp. 11180-, Glasgow, UK, October 2023.

[21] M. Yazdani-Asrami, A. Sadeghi, S. Seyyedbarzegar, and W. Song, "DC Electro-Magneto-Mechanical Characterization of 2G HTS Tapes for Superconducting Cable in Magnet System Using Artificial Neural Networks," IEEE transactions on applied superconductivity, vol. 32, no. 7, pp. 1–10, Glasgow, UK, October 2022.

[22] R. Alizadeh, J. Mohebbi Najm Abad, A. Fattahi, E. Alhajri, and N. Karimi, "Application of Machine Learning to Investigation of Heat and Mass Transfer Over a Cylinder Surrounded by Porous Media—The Radial Basic Function Network," Journal of energy resources technology, vol. 142, no. 11, London, UK, November 2020.

[23] N. M. K. Abdel-Gawad, A. Z. El Dein, and M. Magdy, "Mitigation of induced voltages and AC corrosion effects on buried gas pipeline near to OHTL under normal and fault conditions," Electric power systems research, vol. 127, pp. 297–306, Cairo, Egypt, October 2015.

979-8-3503-7964-8/24/$31.00 ©2024 IEEE